Mapping the Surface Spin Structure of Large Unit Cells: Reconstructed Mn Films on Fe(001)

C. L. Gao,[1] U. Schlickum,[1,*] W. Wulfhekel,[1,2] and J. Kirschner[1]

[1]*Max-Planck-Institut für Mikrostrukturphysik, Weinberg 2, D-06120 Halle, Germany*

[2]*Physikalisches Institut, Universität Karlsruhe (TH), Wolfgang-Gaede Strasse 1, D-76131 Karlsruhe, Germany*

(Received 10 June 2006; published 9 March 2007)

Using spin-polarized scanning tunneling microscopy with ring electrodes, the in-plane spin polarization of Mn on Fe(001) was measured. A large $(\sqrt{10} \times 2\sqrt{10})R18.4°$ reconstruction with a noncollinear spin structure was found. By combining maps of the spin polarization for two orthogonal in-plane directions, the vector field of the polarization in the unit cell could be constructed. The complex behavior is explained on the basis of the tendency of Mn to form antiferromagnetically coupled surface dimers.

DOI: 10.1103/PhysRevLett.98.107203 PACS numbers: 75.70.Ak, 68.35.Bs, 68.37.Ef, 75.50.Ee

Antiferromagnets play an important role in pinning ferromagnets in spin-electronic devices [1,2]. The spin structure of an antiferromagnetic surface is of key importance for the exchange bias effect and is at the heart of understanding the details of the coupling mechanism [3,4]. Often, antiferromagnets with noncollinear spin structures are used in exchange bias applications [5,6]. Therefore, the investigation of noncollinear spin structures of surfaces is not only of fundamental interest but also of importance from the technological point of view. Traditional methods to study antiferromagnets are usually bulk sensitive like neutron diffraction [7,8] and operate in reciprocal space. With the development of spin-polarized scanning tunneling microscopy (Sp-STM), it became possible to study the spin configuration of antiferromagnetic surfaces on the atomic level [9].

In this Letter, we show that using ring shaped electrodes in Sp-STM [10], two well-defined orthogonal in-plane components of an antiferromagnetic spin structure can be recorded. This allows the determination of an in-plane vector map of the spin polarization of noncollinear spin structures. We demonstrate this capability on the example of reconstructed Mn films on Fe(001).

Manganese has the most complex structural and magnetic properties among all elements. The stable bulk α-Mn phase has a cubic unit cell of 58 atoms with a lattice constant of 8.87 Å [7]. Bulk α-Mn shows a noncollinear antiferromagnetic structure [11,12]. Mn also accounts for the various magnetic properties in Mn-based alloys such as FeMn [5] and NiMn [6] which are used as pinning layers in exchange-biased systems. Therefore, Mn was intensively investigated in both bulk [8,13] and thin films [14–17] in the last a few decades. Mn can be stabilized on Fe(001) in a body-centered tetragonal (bct) structure below a critical thickness of 10 to 20 monolayers (ML) which shows a collinear layerwise antiferromagnetic structure [16–18]. It has been proposed that a structural transition from bct Mn to α-Mn [14,15] takes place above this critical thickness. In our study, we focused on Mn films on Fe(001) above the critical thickness.

For the Sp-STM measurements, a ferromagnetic CoFeSiB ring was used as a tip electrode. Because of the magnetic shape anisotropy, the ring has two stable magnetization states, in which the magnetization circles around the center of the ring. At the outer perimeter, the magnetization lies tangential to the ring and in the ring plane, which was aligned with the Fe whisker axis. The tunneling current between the ring and the sample surface depends on the relative orientation of magnetization of the ring and the sample due to the tunneling magnetoresistance effect [19]. In the experiment, the magnetization direction of the ring is switched periodically between the two stable states of opposite magnetization. This is equivalent to periodically reversing the spin polarization of the ring. As a result, the time averaged tunneling current does not depend on the spin of the sample surface and is used to obtain the topography. The difference between the two tunneling currents is proportional to the projection of the sample spin polarization on the ring tangential, i.e., along Fe[100]. In this way, a well-defined in-plane component of the spin polarization of the sample surface can be mapped simultaneously to the topography. Before each measurement, the ring electrode was cleaned by Ar^+ sputtering. We found that on average the spin contrast was enhanced if about 10 ML Fe was deposited on top of the ring electrode. A more detailed description of the technique can be found elsewhere [10].

The experiments were done in ultra high vacuum ($p_{\text{base}} < 1 \times 10^{-10}$ mbar). An Fe whisker was chosen as the substrate due to its simple magnetic domain structure [20]. The whisker was cleaned by cycles of Ar^+ sputtering and annealing to 750 K. Mn was deposited by molecular beam epitaxy while keeping the temperature of the substrate at 373 K. The growth rate was ≈ 0.5 ML per minute as determined from medium energy electron diffraction (MEED) intensity oscillations.

During Mn deposition, we observed a dramatic decrease of the MEED intensity within one ML indicating the structural transition. In the transition region, bct Mn and reconstructed Mn coexist as shown in Fig. 1. In the topographic image (cf. Figure 1(a)], most of the surface is atomically flat. An atomic step runs across the image between two terraces as indicated by the arrow. Our Sp-STM is sensitive to the in-plane spin polarization parallel to the magnetization direction of the ring. The brightness in

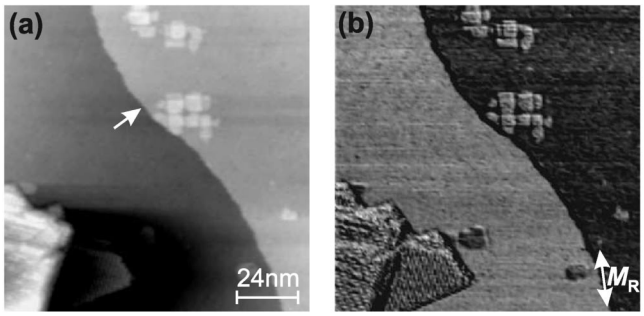

FIG. 1. Sp-STM images of (a) the topography and (b) the spin signal of 11 ML Mn on Fe(001) ($U = 0.1$ V, $I = 3$ nA). The atomically flat terraces in (a) are bct Mn separated by an atomic step (arrow). An antiferromagnetic spin contrast between neighboring atomic layers was observed in (b). The island in the left-bottom part is reconstructed. M_R shows the magnetization direction of the ring.

the spin images reflects the spin polarization projected to the ring direction. In the corresponding spin channel in Fig. 1(b), a strong contrast between the two bct Mn terraces was observed, which reflects the layerwise antiferromagnetic order of bct Mn [17]. The topographic image of Fig. 1(a) shows a reconstructed island with periodic features on it in the bottom-left corner. Obviously, the reconstruction of Mn starts as islands with a typical height between 0.5 nm and 1.5 nm. In the spin signal (cf. Figure 1(b)], a regular pattern was seen, suggesting that the reconstructed Mn atoms show magnetic moments as well [21].

Low energy electron diffraction (LEED) was used to characterize the structure of the Mn films. While a sharp (1×1) LEED pattern was observed below the transition, a $(\sqrt{10} \times 2\sqrt{10})R18.4°$ was seen above (cf. Figure 2(a)]. It contains four subpatterns. The size of the unit cell is $a = 9.06$ Å, $b = 18.12$ Å, i.e., twice as large as the α-Mn(001) unit cell. In the STM topography (cf. Figure 2(b)], the reconstruction is characterized by parallel lines of protrusions (white), which are separated by ~18 Å. The distance between two protrusions within one line is ~9 Å. The four LEED subpatterns correspond to parallel lines running along [130], [$\bar{1}$30], [310], and [$\bar{3}$10] directions [22]. As can be seen from Fig. 2(b), some protrusions in the top layer are missing, such that the layer below is visible. This allows us to estimate the atomic layer thickness of the reconstruction to about 1 Å. There are between 14 and 15 Mn atoms in the volume of 9 Å × 18 Å × 1 Å taking the packing density of α-Mn. This block is the growth unit and about half of the Wigner-Seitz cell of α-Mn.

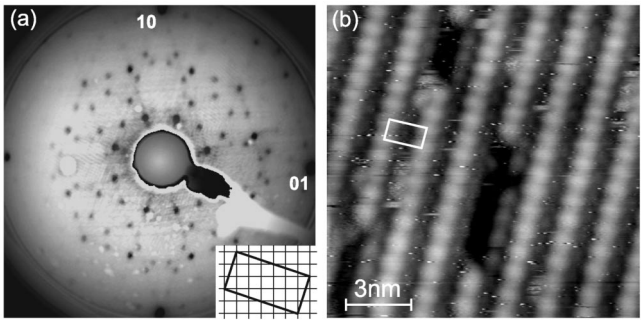

FIG. 2. (a) 33.6 eV LEED pattern of 14 ML Mn on Fe(001). The inset shows the unit cell with respect to the Fe lattice in real space. (b) STM image of the reconstructed Mn taken with a W tip ($U = 0.5$ V, $I = 1$ nA).

The structure and spin configuration within the unit cell was visible when zooming into those islands. Figure 3(a) shows the topography recorded with a ring electrode. The resolution is not fully atomic and is lower than that of Fig. 3(b), which was taken with a W tip showing atomic resolution. We attribute this difference in resolution to the higher focusing of electronic tip states in W than in Fe, as was shown by *ab initio* calculations [23]. As indicated by the white arrow in Fig. 3(b), the protrusions consist of at least three atom pairs in a row. The lateral positions of the atoms within the reconstruction indicate a tendency for dimer formation. In case the surface atoms order antiferromagnetically, the periodicity of the spin polarization is at least twice as large as the periodicity of the topographic structure. Therefore, it is easier to resolve single spins in

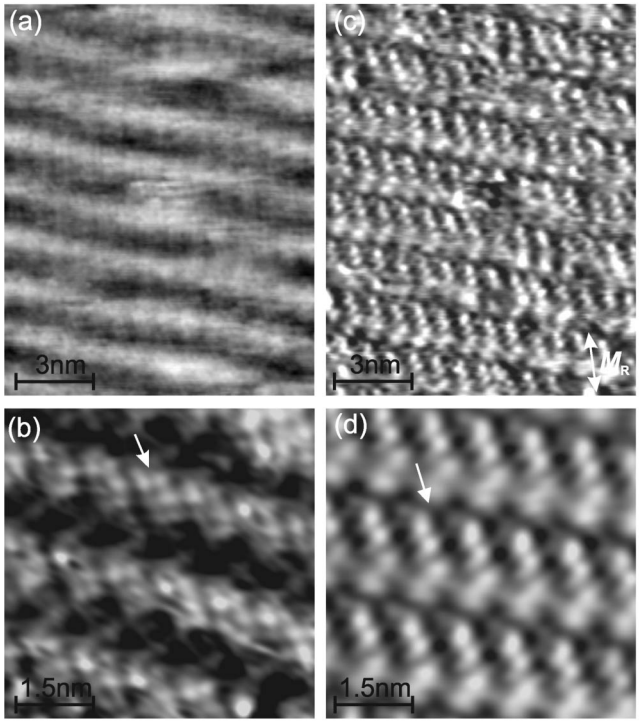

FIG. 3. High resolution Sp-STM images of (a) the topography and (c) the spin signal of the reconstructed Mn surface ($U = 0.1$ V, $I = 3$ nA). (b) the atomically resolved image taken with a W tip ($U = 0.03$ V, $I = 25$ nA). (d) The averaged spin image over many unit cells of (c). M_R shows the magnetization direction of the ring.

antiferromagnets than single atoms [9]. Figure 3(c) is the atomically resolved spin image taken simultaneously with the topography of Fig. 3(a) [24]. The ring electrode was arranged along Fe[100], i.e., close to perpendicular to the reconstruction lines and parallel to the dimer rows. The individual dimers appear as pairs of white and black dots in the spin image, which implies a nearly antiparallel alignment of magnetic moments within the dimers, while neighboring dimers within the rows are oriented in parallel. This becomes more obvious when averaging over many unit cells to reduce the noise (cf. Figure 3(d)]. As indicated by the arrow in Fig. 3(d), the positions and distance of these dimers in the spin signal fit well to the structurally correlated dimers as shown in Fig. 3(b). The high contrast in the spin signal (white and black dots) suggests that these atoms correspond to high spin Mn atoms. The bulk terminated α-Mn(001) surface exposes six high spin atoms in the area of 9 Å $\times$ 18 Å. However, the positions of these high spin atoms do not agree with the positions of the high spin atoms as observed with Sp-STM. This indicates that the reconstruction involves a reconfiguration of the surface atoms with respect to bulk α-Mn. When taking into account the partly covalent nature of the Mn-Mn bond in α-Mn [7,13], an open surface leaves dangling Mn bonds behind. To saturate these, it is likely that the surface Mn atoms form dimers. This not only explains the observed dimers in the topographic images, it also gives a reason for the nearly antiparallel alignment of the moments and the high contrast in the spin image. The atoms of the dimers need an antiparallel magnetic coupling to form a covalent bond (neglecting the bonds to the subsurface atoms).

To find out, if the spin structure at the surface is a collinear or a noncollinear one, Sp-STM images with different orientations of the reconstruction lines with respect to the ring were taken. Figs. 4(a) and 4(b) show the spin images of two structural domains with perpendicular orientations of the reconstruction lines and same ring orientation. The spin images show the same periodicity as Fig. 3(d) but give less detailed information. Note that it was necessary to cut the two spin images from one larger image of lower resolution to guarantee the same tip apex and to allow direct comparison of the spin signals. There are no differences in the topography (not shown here) except for the orientations of the two domains. However, in the spin channel, the two domains differ. In Fig. 4(a), the ring was close to perpendicular to the lines similar to Fig. 3(d). Figure 4(a) is characterized by bright dots forming bright lines and well separated gray dots between the bright lines while Fig. 3(d) shows two bright dots and two less bright dots below them. In both Figs. 3(d) and 4(a), the positions of intermediate spin signal correspond to topographic positions between the reconstruction lines. Figure 4(a) is consistent with Fig. 3(d) but gives less detail [25]. In Fig. 4(b), the ring was close to parallel to the lines. The image is characterized by well ordered bright dots

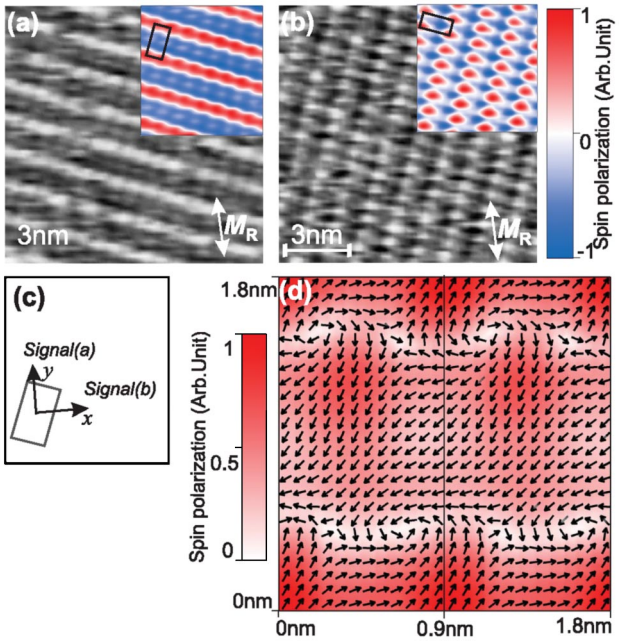

FIG. 4 (color). (a) and (b) are spin images of two perpendicular domains of the reconstructed Mn ($U = 0.1$ V, $I = 3$ nA). The unit cell of 9 Å $\times$ 18 Å is indicated in the images. The insets represent averaged unit cells. M_R shows the magnetization direction of the ring. (c) sketches the way of combining image (a) and (b). Signal(a) and Signal(b) represent the signal of inset images in (a) and (b). Image (b) is rotated by 90° to fit with image (a). (d) gives the spin distribution of two reconstruction unit cells of 9 Å $\times$ 18 Å each. The white-red coded intensity represents the absolute magnitude of the in-plane spin polarization. The directions of the arrows give the directions of the in-plane spin polarization.

forming a rectangular shape. When comparing the spin signals of two unit cells (cf. insets of Figs. 4(a) and 4(b)], one realizes that they do not show the same pattern which is a necessary condition for a collinear spin arrangement. There are two possibilities that could explain the differences in the spin structure. First, the two domains have different spin configurations due to their different orientations with respect to the underlying Fe whisker magnetization. Second, the unit cell has a noncollinear spin structure not related to the underlying Fe. In order to distinguish between the two possibilities, we rotated the ring by 90° with respect to the Fe whisker magnetization. The resulting spin images revealed that when the ring is perpendicular to the reconstruction lines, the spin image is similar to Fig. 4(a) while the spin image is similar to Fig. 4(b) when the ring is parallel to the lines (not shown). This means that the spin images depend only on the direction of the ring with respect to the direction of the reconstruction and not on the direction of the Fe whisker. Therefore, the magnetic structure of the reconstructed Mn is dominated by the structure itself. As a consequence of this, Mn must have a noncollinear spin structure. The noncollinear antiferromagnetic structure of the recon-

structed Mn surface is not surprising since the superstructure is similar to a doubled α-Mn unit cell while bulk α-Mn has a complex noncollinear spin structure [8]. Since the reconstruction lines in Figs. 4(a) and 4(b) were perpendicular, the two images represent two orthogonal components of the spin polarization of the unit cell. The averaged spin signal within the unit cell is zero, i.e., the spin structure is compensated, as was deduced from the absence of any large scale spin contrast between different reconstruction domains and terraces. Taking the spin-polarization within the unit cell of the inset of Fig. 4(a) as y component [signal(a)] and that of Fig. 4(b) as x component [signal(b)] as sketched by Fig. 4(c), the two spin images can be combined to a vector map. The resulting vector map is given in Fig. 4(d). Both the size and the direction of the in-plane spin polarization vary within the unit cell as indicated by the white-red coded background and the black arrows in Fig. 4(d). Clearly, the spin distribution within the unit cell deviates from a collinear configuration. Because of the limited lateral resolution of the combined scan of about 5 Å, the vector plot does not resolve the drastic change of spin polarization within the dimers. Figure 4(d), however, still reveals the complexity and noncollinearity of this reconstructed α-Mn. The antiferromagnetically coupled surface dimers and the noncollinear surface spin structure both indicate a tendency of the surface to form an in-plane compensated spin structure. This may be essential to understand the relatively moderated size of the exchange bias effect in ferromagnetic/antiferromagentic layers.

In conclusion, we have investigated the structure of $(\sqrt{10} \times 2\sqrt{10})R18.4°$ reconstructed Mn on Fe(001) with LEED and STM. The noncollinear spin configuration of the surface atoms in the unit cell was mapped with Sp-STM. The spin structure was explained on basis of the tendency of Mn to form covalent dimer bonds at the surface leading to a locally antiparallel orientation of the moments. Together with the complex crystallographic structure, this results in a noncollinear spin configuration. The mechanism is expected to be responsible for the wide variety of spin structures in Mn alloys. This work illustrates the capability of Sp-STM with ring electrodes to map the surface spin polarization. In contrast to thin film coated tips, the magnetization direction of ring electrodes is well-defined, and a vector map can be constructed without directional uncertainties.

*Present address: Institut de Physique des Nanostructures, EPFL, CH-1015 Lausanne, Switzerland

[1] G. A. Prinz, Science **282**, 1660 (1998).
[2] S. A. Wolf, D. D. Awschalom, R. A. Buhrman, J. M. Daughton, S. von Molnár, M. L. Roukes, A. Y. Chtchelkanova, and D. M. Treger, Science **294**, 1488 (2001).
[3] R. L. Stamps, J. Phys. D **33**, R247 (2000).
[4] A. P. Malozemoff, Phys. Rev. B **35**, 3679 (1987).
[5] W. Kuch, L. I. Chelaru, F. Offi, J. Wang, M. Kotsugi, and J. Kirschner, Nat. Mater. **5**, 128 (2006).
[6] K. Nakamura, A. J. Freeman, D. S. Wang, L. Zhong, and J. Fernandez-de-Castro, Phys. Rev. B **65**, 012402 (2001).
[7] T. Yamada, N. Kunitomi, Y. Nakai, D. E. Cox, and G. Shirane, J. Phys. Soc. Jpn. **28**, 615 (1970).
[8] A. C. Lawson, Allen C. Larson, M. C. Aronson, S. Johnson, Z. Fisk, P. C. Canfield, J. D. Thompson, and R. B. Von Dreele, J. Appl. Phys. **76**, 7049 (1994).
[9] S. Heinze, M. Bode, A. Kubetzka, O. Pietzsch, X. Nie, S. Blügel, and R. Wiesendanger, Science **288**, 1805 (2000).
[10] U. Schlickum, W. Wulfhekel, and J. Kirschner, Appl. Phys. Lett. **83**, 2016 (2003).
[11] R. S. Tebble and D. J. Craik, *Magnetic Materials* (Interscience, London, 1969).
[12] H. Yamagata and K. Asayama, J. Phys. Soc. Jpn. **33**, 400 (1972).
[13] D. Hobbs, J. Hafner, and D. Spišák, Phys. Rev. B **68**, 014407 (2003).
[14] S. Andrieu, M. Finazzi, Ph. Bauer, H. Fischer, P. Leferve, A. Traverse, K. Hricovini, G. Krill, and M. Piecuch, Phys. Rev. B **57**, 1985 (1998).
[15] E. C. Passamani, B. Croonenborghs, B. Degroote, and A. Vantomme, Phys. Rev. B **67**, 174424 (2003).
[16] T. K. Yamada, M. M. J. Bischoff, G. M. M. Heijnen, T. Mizoguchi, and H. van Kempen, Phys. Rev. Lett. **90**, 056803 (2003).
[17] U. Schlickum, N. Janke-Gilman, W. Wulfhekel, and J. Kirschner, Phys. Rev. Lett. **92**, 107203 (2004).
[18] T. G. Walker and H. Hopster, Phys. Rev. B **48**, 3563 (1993).
[19] M. Julliére, Phys. Lett. A **54**, 225 (1975).
[20] A. Hubert and R. Schäfer, *Magnetic Domains: The Analysis of Magnetic Microstructures* (Springer, Berlin, 1998).
[21] Note that there is a cross talk from the topography into the spin signal at step edges partly due to the limited bandwidths of the feedback loop. We can, however, exclude this effect on the reconstructed islands (50 pm corrugation) because the spin signal is independent of the scanning direction and it is not related to areas of maximal topographic corrugation.
[22] Note that in the hundreds of domains observed with STM, none of the domains showed a different structure, and none of the films displayed a different LEED pattern. The features presented are therefore characteristic of the reconstruction.
[23] W. A. Hofer, J. Redinger, and R. Podloucky, Phys. Rev. B **64**, 125108 (2001), and references therein.
[24] Note that in only 10% of the experiments atomic resolution similar to Fig. 3(c)] was obtained.
[25] When the atomically resolved spin image of Fig. 3(d) is numerically blurred along the lines with a Gaussian of 5 Å width, it agrees well with the image of Fig. 4(a).